JOURNAL OF PROPULSION AND POWER
Vol. 17, No. 2, March–April 2001

Upstream-Propagating Potential Disturbances Interacting with A Compressible Cascade

Michael K. Fabian*
U.S. Air Force Academy, Colorado Springs, Colorado 80840
and
Eric A. Falk† and Eric J. Jumper‡
University of Notre Dame, South Bend, Indiana 46556

Phase-locked, unsteady surface-pressure measurements were made at eight suction-side and six pressure-side chord locations on the turning vanes of a compressible cascade. Cascade inlet Mach numbers ranged from 0.427 to 0.500, resulting in a maximum local Mach number through the cascade vane row of 0.730. Unsteady forcing of the cascade was obtained by von Kármán vortex shedding from a row of five circular cylinders positioned 0.80 vane chords downstream of the cascade trailing edge. The resulting measured surface pressures were found to be on the same order of magnitude as those measured previously in forward-forcing studies, in which the circular cylinders were placed 0.80 vane chords upstream of the vane-row leading edge. Frequency decomposition of the rearward-forced surface-pressure signals provided for the construction of disturbance position-vs-phase maps, allowing the measured disturbances to be unambiguously interpreted as potential in nature, originating at the forcing cylinders, and propagating upstream through the vane row at acoustic speeds. The effect of these potential disturbances on the vane-row pressure response was to elicit two, previously unexpected amplification mechanisms: a large-magnitude pressure rise near the vane-row trailing edge and a Mach-number-related, midchord pressure increase known as acoustic blockage.

Nomenclature

A = amplitude
a = speed of sound
c = stator chord
d = forcing-cylinder diameter
f = frequency
L = lift
M = Mach number
P = pressure
r = cylindrical coordinate
T = period of circulation fluctuation
t = time
V = velocity
x = linearized r coordinate
y = linearized θ coordinate
Γ = cylinder bound circulation
θ = cylindrical coordinate
ρ = air density
ϕ = measured/decomposed phase
φ = analytical model phase
ω = angular frequency

Subscripts

D = drag component
h = harmonic-frequency component
L = lift component
p = primary-frequency component
pr = pressure surface
s = suction surface
0 = initial property
∞ = freestream component

Superscripts

$\hat{}$ = unit vector
$'$ = unsteady property
$\bar{}$ = average property
$\tilde{}$ = unmeasured property

Received 13 August 1999; revision received 5 January 2000; accepted for publication 9 June 2000.

*Assistant Professor, Department of Aeronautics, HQ USAFA/DFAN. Member AIAA.

†Graduate Research Assistant, Department of Aerospace and Mechanical Engineering, Hessert Center for Aerospace Research. Student Member AIAA.

‡Professor, Department of Aerospace and Mechanical Engineering, Hessert Center for Aerospace Research. Associate Fellow AIAA.

Introduction

HIGH-CYCLE fatigue (HCF) in a turbomachine compressor is a structural failure mode in which the compressor blade/vane components, exposed to prolonged cyclic loading, may experience crack formation, or even catastrophic failure. To predict compressor HCF failure, a considerable amount of experimental and computational research has historically been performed; however, failures of this type continue and are almost exclusively unexpected. In fact, turbomachine failures related to HCF are known to be a major contributor to engine-safety mishaps in military fighter aircraft and therefore remain a major readiness concern for the U.S. Air Force and U.S. Navy.[1] These readiness concerns have recently prompted the U.S. Department of Defense to established the National Turbine Engine High-Cycle Fatigue Program, which has the stated goal of identifying, and eliminating, factors leading to HCF engine failure. One component of the HCF Program is directed toward improved forced-response prediction, necessarily requiring an improved understanding of the aerodynamic forcing functions that drive many HCF problems.

Aerodynamic forcing functions in turbomachine compressors have been traditionally considered to be caused by the vortical wakes developed by each upstream compressor stage. These wakes are convective and elicit an unsteady forced response from the downstream blade/vanes they encounter. Such a traditional view of aerodynamic forcing, however, does not provide a complete picture of the total forcing environment, as other, unaccounted for, forcing mechanisms may contribute to the continual occurrence of unpredicted HCF failures.[1] In fact, recent investigations have shown that the forcing

environment, at a minimum, also includes the effects of propagating, unsteady potential disturbances, particularly upstream-propagating potential disturbances.

Schmidt and Okiishi[2] were among the first to consider the effects of upstream-propagating potential disturbances on compressor aerodynamic forcing. Their experiment was performed in a low-speed compressor rig and, like many examinations to follow,[3–6] considered simultaneous downstream and upstream forcing. As such, these previous studies drew essentially no conclusions regarding the relative importance of downstream forcing. More recent investigations, like those of Johnston and Fleeter[7,8] and Hsu and Wo,[9] have specifically examined the effect of upstream-propagating disturbances on rotor/stator interactions, in both high-speed and low-speed compressor rigs. These experiments have shown upstream-propagating potential disturbances to significantly alter the character of downstream-propagating, vortical forcing functions. In addition, Probasco et al.[10,11] examined the effect of upstream-propagating potential disturbances on inlet-guide-vane (IGV) surface-pressure response forward of a supersonic fan, where the IGV was unloaded, designed with a rounded trailing edge, and the forcing disturbances were shock induced. From their results they concluded that the IGV pressure response, caused by potential forcing, was of first-order importance to the rotor/stator interaction problem.

Although these previous rotating-machine experiments have examined compressor potential field interactions, no study has isolated an upstream-propagating potential disturbance in a simplified flow configuration, i.e., without rotating components. Moreover, the effect of a propagating potential disturbance on stator-vane pressure response has yet to be determined, specifically for vanes with a sharp trailing edge, high aerodynamic loading, and subsonic flow conditions.

In a previous paper[12] we investigated isolated, upstream-propagating potential disturbances interacting with a sharp-trailing-edge vane row in an unsteady, loaded transonic cascade. This paper provided three important results. First, it established the flow quality of the cascade; the cascade flow was shown to be fully attached, essentially two-dimensional, and periodic over the Mach numbers tested.[12] Second, the paper demonstrated the importance of rearward forcing, as the unsteady-pressure response of the cascade vanes was found to be on the same order as that of the forward-forced cascade. Finally, the paper introduced a simple, analytical disturbance-propagation model, from which it was possible to examine the forcing disturbance characteristics, through the interpretation of disturbance position-vs-phase maps.

The present paper is a companion to our previous article.[12] As such, this paper only briefly describes the cascade facility and data-collection techniques, depending heavily on Ref. 12; however, the paper does provide additional experimental results to those of Ref. 12. The main contribution of the current paper is a description of the cascade aerodynamic forcing mechanisms, providing physical meaning for the two separate frequency components observed in the measured pressure-response data. This description of the forcing allows us to examine two new pressure-response amplification mechanisms that appear in the measured pressure-response data, in particular, a large unsteady pressure disturbance at the vane trailing edge and acoustic blockage.

Facilities and Equipment

The Notre Dame cascade forms the test section of a transonic, in-draft wind tunnel located at the Hessert Center for Aerospace Research.[12–14] This tunnel is powered by three 1.562 m^3/s Allis-Chalmer vacuum pumps, and the cascade is formed by six stator vanes: four midstream and two wall vanes, forming five equally spaced flow passages, as shown in Fig. 1. The cascade inlet and outlet cross-sectional areas are both 10.16×10.16 cm.

Cascade Turning Vanes

The cascade turning vanes are production-hardware stator vanes taken from the single-stage axial compressor in a General Electric (AlliedSignal) F109 turbofan engine. The vanes have a double-circular-arc airfoil section, with a maximum camber and thickness

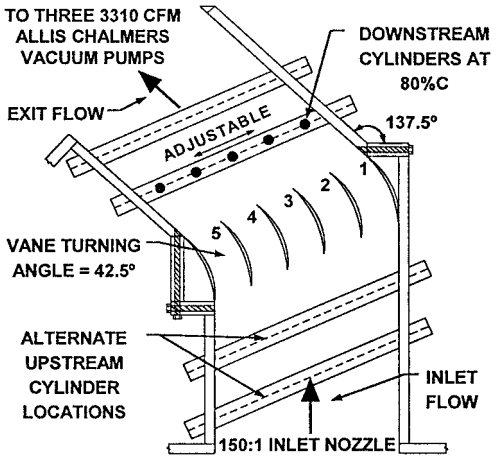

Fig. 1 Top view of cascade test section.

of 0.12 and 0.08 vane chords, respectively. The nominal chord of the vanes in the streamwise cascade direction is 3.25 cm, with a vane spacing of 2.13 cm. The cascade turning angle is 42.5 deg, as shown in Fig. 1, with a stagger angle of −9 deg and no diffusion, as required to maintain attached flow over the cascade vanes (see Ref. 12). In the F109 the vanes are swept aft from hub to tip; however, in the cascade the vanes are mounted vertically to form a two-dimensional linear cascade. Such a cascade configuration is not intended to duplicate the F109 stator-vane row, but rather to provide a simplified flow configuration that approximates the flow through an axial-flow compressor stage.[12]

Sixteen vanes were instrumented with surface-mounted, Kulite XCS-062 ultraminiature transducers along two streamwise axes, where these two axes are denoted engine-axis 1 and engine-axis 2 (Ref. 12). Because of the thin geometry of the vanes, the transducers were limited to eight chord locations between 0.07 and 0.80 vane chords. Similarly, space limitations allowed only two transducers per vane; each vane was instrumented with one pressure-surface and one suction-surface transducer. The Kulite transducers have a flat dynamic response in excess of 20 kHz (Ref. 12).

Unsteady Forcing

Cascade unsteady forcing was established through von Kármán vortex shedding from a row of five circular cylinders. The cylinders could be placed either upstream or downstream of the cascade vanes at 0.80 or 1.60 vane chords from the leading or trailing edge of the vane row (Fig. 1 shows the cylinders in the downstream 0.80 vane-chord position). The forcing cylinders were aligned normal to the oncoming flow, parallel to the vane span direction, with the cylinder spacing equal to the vane spacing. No active control of the cylinder shedding was used; all five cylinders were found to shed in phase.[12–14]

The results presented here are from rearward forcing along engine-axis 2. The cylinders were positioned 0.80 vane chords downstream and aligned in the cross-stream direction with the vane midpassage location. The cylinder diameters were 4.7 mm, yielding a reduced frequency based on vane half-chord of 4.5 over the tested inlet Mach numbers. The inlet Mach numbers were limited between 0.427–0.500 because of the cylinder unsteady-forcing mechanism[12]; however, this represents a relatively large change in operating conditions within the F109 engine, from which the stator vanes were obtained.[14]

Phase-Locked Data Acquisition

Unsteady surface-pressure measurements were acquired through conditional sampling techniques based on the initiation of a trigger signal. Trigger initiation occurred when a transducer embedded in one of the forcing cylinders obtained a minimum pressure amplitude on the surface of the cylinder, caused by vortex shedding.[12] The shedding periodicity was sufficient to provide ensemble-averaged results, as well as to determine the unsteady

aerodynamic characteristics of the flow. Each trigger initiation allowed a single data set to be collected. A total of 400 data sets were acquired at each transducer location and Mach number, allowing phase-locked ensemble averaging of the pressure signals.[12–14] Data were collected with the instrumented stator vanes placed at the same relative location across the cascade vane row for all measurements.

A number of steady-state (unforced) cascade tests were initially performed to verify the cascade flow quality and transducer reliability. The details of this flow quality and instrumentation verification are not presented here in detail but are fully described in Ref. 12. It is noted, however, that the steady cascade flow was found to be essentially two-dimensional and attached over the instrumented region of the vanes. Additionally, the unsteady cascade flow was observed to be repeatable and sufficiently periodic across the vane row, conforming to the periodicity conditions set forth by Oates[15] for subsonic surface-pressure measurements.[12] The Kulite transducers were found to be reliable, showing no abnormal behavior.[12] Static and total pressures were measured upstream of the vane row, allowing the vane row, inlet Mach number, and static pressure to be computed. Further details on the data acquisition are given in Ref. 12.

Pressure-Response Data Reduction

Two data-reduction techniques were employed on the measured pressure-response data. First, the 400 phase-locked data sets collected at each chordwise position and Mach number were ensemble averaged. Second, following the example of previous stator-response data,[5] the ensemble-averaged data were frequency decomposed into primary and harmonic sinusoidal signals using the decomposition routine described in Ref. 14.

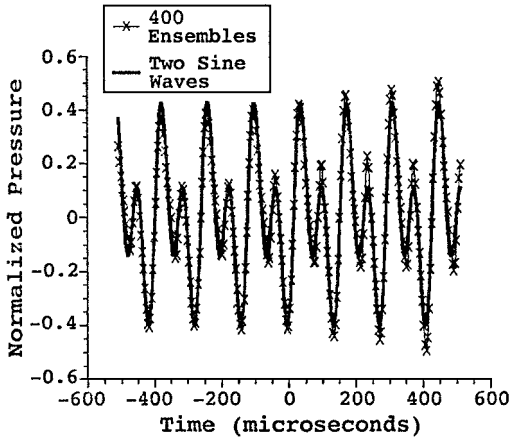

Fig. 2 Representative two sine-wave unsteady pressure signal reconstruction.

The decomposition routine converges on a global-optimum six-parameter fit to the 400-ensemble response data. The amplitude, frequency, and phase for both primary and harmonic frequency sine-wave signals were optimized, with the function

$$P' = A_P \sin(2\pi f_p t + \phi_p) + A_h \sin(2\pi f_h t + \phi_h) \qquad (1)$$

selected as the merit function to be compared against the measured unsteady-pressure signals. The routine minimized the rms error between Eq. (1) and the measured data. A reconstruction of a measured unsteady-pressure signal, using Eq. (1) for an inlet Mach number of 0.427 at the suction-surface 0.30 vane-chord location, is shown in Fig. 2 (Ref. 12). The average rms error between a reconstructed and measured unsteady-pressure signal was approximately 400 Pa, where the nominal primary-frequency amplitude of the measured pressure, for all inlet Mach numbers considered, was approximately 2400 Pa (Ref. 12).

Table 1 provides the entire decomposed, 0.475 inlet-Mach-number data set, given in terms of normalized amplitude, frequency, and phase, for the primary and harmonic frequencies (normalizing amplitude = 2075 Pa). This table provides, through Eq. (1), a complete set of unsteady pressure-response data for the 0.475 inlet-Mach-number case.

Before continuing, a few notes on experimental error should be made. First, under the assumption that the variation of any, individual, pressure-response data set from its corresponding 400-ensemble set is random, the 400-ensemble set represents the true expected signal. The ensemble-averaging process essentially removes the random component from the measured data. Second, the use of 400 ensembles was found to give less than 0.1% rms error relative to 1000 ensembles. Therefore, the error of the data presented here, relative to the true expected signal, consists primarily of the rms error associated with the decomposition-routine reconstruction, as just mentioned.[12] Additional bias errors, caused by instrumentation, are also present; however, these bias errors are smaller than the data-point symbols reported in the following figures. Specific details on the cascade experimental error can be found in Refs. 12 and 14.

Nature of the Forcing Disturbance

Using the decomposed, unsteady pressure-response data of Table 1, it was possible to examine specific aspects of the rearward-forced data. For example, as was done in Ref. 12 for the 0.427 inlet-Mach-number case, plots of the primary and harmonic frequency components of the decomposed pressure-response phase for 0.475 inlet-Mach-number case could be constructed, as given in Figs. 3 and 4. Figures 3 and 4 indicate the phase of the unsteady-pressure response along the suction and pressure surfaces of the nominal

Table 1 Decomposed amplitude, frequency, and phase for $M = 0.475$, engine-axis 2, rearward-forced data (normalizing amplitude = 2075 Pa)

x/c position	Primary amplitude (norm.)	Harmonic amplitude (norm.)	Primary frequency, Hz	Harmonic frequency, Hz	Primary phase, rad	Harmonic phase, rad
0.07 suction	0.160	0.057	8,532	17,895	−8.046	−38.320
0.13 suction	0.182	0.089	8,581	17,424	−6.574	−35.284
0.21 suction	0.363	0.171	8,628	17,273	−6.381	−32.840
0.30 suction	0.819	0.140	8,630	17,441	−4.848	−31.427
0.39 suction	0.777	0.337	8,631	17,324	−3.815	−28.210
0.50 suction	0.793	0.220	8,630	17,274	−2.672	−26.105
0.66 suction	0.799	0.153	8,647	17,302	−0.834	−22.002
0.80 suction	1.000	0.191	8,617	17,246	−0.307	−17.502
0.08 pressure	0.366	0.090	8,594	17,082	−8.511	−39.014
0.21 pressure	0.367	0.252	8,474	17,287	−6.271	−35.610
0.30 pressure	0.344	0.339	8,270	17,320	−4.734	−34.020
0.40 pressure	0.436	0.450	8,732	17,263	0.403	−27.231
0.49 pressure	0.217	0.314	9,382	17,296	−0.288	−24.949
0.64 pressure	0.266	0.399	9,263	17,305	0.737	−22.766
0.79 pressure	0.157	0.233	8,805	17,237	2.579	−15.230

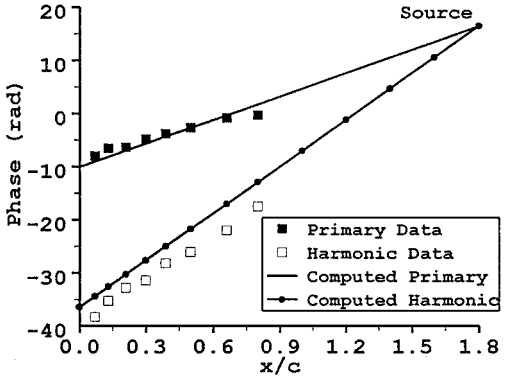

Fig. 3 Suction-surface upstream-traveling wave vs primary and harmonic phase, inlet $M = 0.475$.

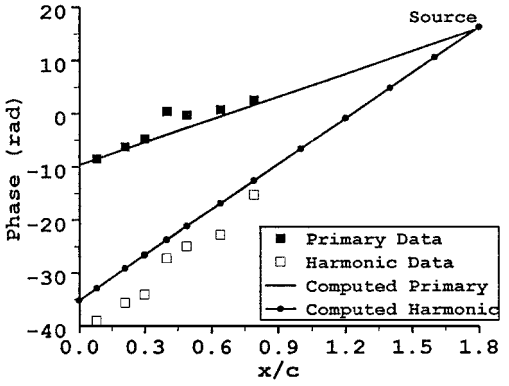

Fig. 4 Pressure-surface upstream-traveling wave vs primary and harmonic phase, inlet $M = 0.475$.

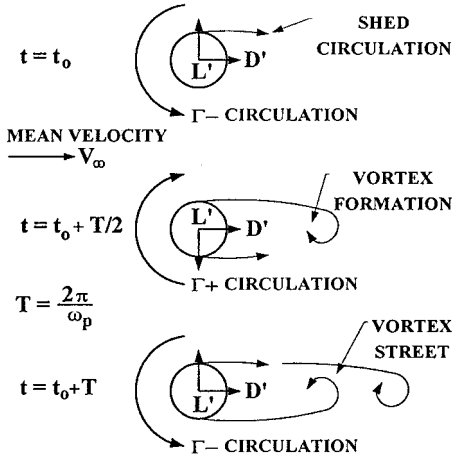

Fig. 5 Schematic of cylinder vortex shedding.

vane, for the 0.475 inlet-Mach-number case. Also shown in Figs. 3 and 4 are analytically computed solid lines indicating the theoretical phase delay of the pressure disturbances from their source to the leading edge of the vane. These lines were computed using the disturbance-propagation model introduced in Ref. 12.

It was argued in Ref. 12 that the relatively good agreement between the 0.427 inlet-Mach-number phase data and the propagation model, similar to the agreement shown in Figs. 3 and 4, indicated that the measured disturbances were propagating upstream through the vane row from trailing edge to leading edge, originating at the forcing cylinders. However, in Ref. 12 a discussion of the propagation model was omitted. Therefore, in order to provide a better understanding of the rearward-forced pressure-response data, the propagation model is discussed here.

It can be assumed, given the forcing-cylinder arrangement in the cascade, that the measured, unsteady surface-pressure disturbances are associated with the cylinder vortex shedding. For example, as vortices are shed into the cylinder wake, periodically oscillating bound circulation is formed around the cylinder, as illustrated in Fig. 5. This oscillating bound circulation is always equal and opposite to the circulation of the alternating-sense wake vortices, and therefore produces a sinuous lift on the cylinder approximately equal to

$$L' = \rho_\infty V_\infty \Gamma \sin(\omega_p t) \tag{2}$$

The lift in Eq. (2) cycles between negative, positive, and back to negative for each pair of alternating-sense vortices shed into the wake, as shown in Fig. 5, where the oscillation frequency is equal to the primary forcing frequency in the cascade.

The cylinder vortex shedding also manifests itself as a drag fluctuation that occurs at twice the frequency of the lift oscillations. For each pair of alternating-sense vortices shed into the wake, the cylinder experiences two, essentially identical drag oscillations, i.e., the cylinder experiences an increase in drag for each vortex shed into the wake. Thus, the cylinder drag fluctuations occur at twice the frequency of the lift oscillations or at the harmonic forcing frequency.

Lift-Induced Disturbance Model

The unsteady velocity field produced upstream of the forcing cylinders can be modeled by a cylinder in a uniform flow, where flow unsteadiness is produced by oscillating bound circulation, or lift, on the cylinder. An idealization of this unsteady velocity field, in a uniform incompressible flow, can be written in cylindrical coordinates as

$$\boldsymbol{V}_L = \left[V_\infty\left(1 - \frac{d^2}{r^2}\right)\cos\theta\right]\hat{r} - \left[V_\infty\left(1 - \frac{d^2}{r^2}\right)\sin\theta + \frac{\Gamma}{2\pi r}\sin(\omega_p t)\right]\hat{\theta} \tag{3}$$

where the second term of the $\hat{\theta}$ component simulates the effect of the oscillating cylinder lift. Sufficiently far from the cylinder, where $r \gg d$ along a ray directly upstream (i.e., along $\theta = 0$ deg), the velocity field of Eq. (3) approaches

$$\boldsymbol{V}_L \approx V_\infty \hat{r} - (\Gamma/2\pi r)\sin(\omega_p t)\hat{\theta} \qquad \text{where} \quad r \gg d;\ \theta = 0\,\text{deg} \tag{4}$$

Equation (4) shows that the effect of cylinder lift far upstream is an unsteady, or time-dependent, velocity disturbance, as depicted in Fig. 6. These lift-induced velocity disturbances cycle at the primary forcing frequency, having a strength proportional to the bound circulation and distance upstream. Considering only the unsteady

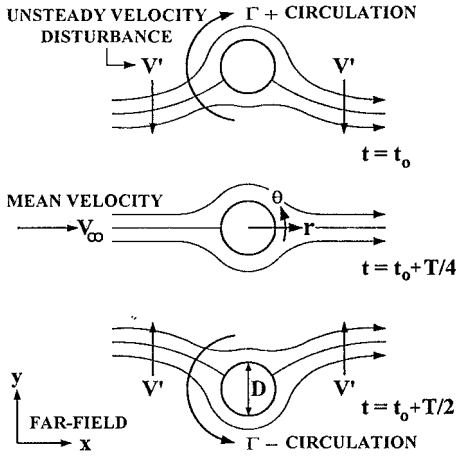

Fig. 6 Schematic of cylinder, alternating bound circulation, with streamlines shown.

portion of the velocity field, the lift-induced disturbances can be further reduced to

$$\boldsymbol{V}'_L \approx -(\Gamma/2\pi r)\sin(\omega_p t + \varphi_p)\hat{\theta} \qquad \text{where} \quad r \gg d;\ \theta = 0\ \text{deg} \tag{5}$$

Note in Eq. (5) that a phase term has been introduced, where this term is associated with the upstream propagation of a disturbance into a compressible flow. In a compressible flow a disturbance requires a finite amount of time to propagate forward to an upstream location because of the local speed of sound. In terms of phase, this time delay exhibits itself as a phase-lag, dependent on the frequency, propagation distance, speed of sound, and Mach number of the flow. Such a phase lag can be written as

$$\varphi_p = \varphi_0 - \frac{\omega_p r}{\bar{a}_{s,\mathrm{pr}}(1 - \bar{M}_{s,\mathrm{pr}})} \tag{6}$$

where the second term on the right-hand side represents a upstream-propagating disturbance traveling at the average acoustic speed $\bar{a}_{s,\mathrm{pr}}$ into an average local Mach number $\bar{M}_{s,\mathrm{pr}}$ over the suction or pressure side of the vane, as applicable.

Drag-Induced Disturbance Model

As with the lift, the drag-induced disturbance field can be modeled as a velocity fluctuation as a result of the cylinder drag oscillations created by the periodic vortex shedding. An increase in cylinder drag, during a given drag oscillation cycle, would have the effect of decreasing the cascade axial velocity below its mean value. Similarly, a decrease in cylinder drag, during the same drag oscillation cycle, would have the effect of increasing the cascade axial velocity above its mean value. The overall effect of the drag oscillations, therefore, would be to create a sinuous, axial velocity fluctuation in the cascade, where these velocity fluctuations would occur at the harmonic frequency of the cylinder forcing (i.e., twice the frequency of the fluctuations caused by the lift oscillations).

The fluctuating velocity field, caused by the cylinder drag, can be written approximately as

$$\boldsymbol{V}'_D = \tilde{V}_D \sin(\omega_h t + \varphi_h)\hat{r} \qquad \text{where} \quad r \gg d;\ \theta = 0\ \text{deg} \tag{7}$$

As before, a phase term has been included in Eq. (7) to simulate the effect of finite upstream-propagation speeds for a disturbance in a compressible flow. Because the drag fluctuations experience the same phase lag as the lift-induced disturbances caused by the compressibility, the phase term in Eq. (7) can be given as

$$\varphi_h = \varphi_0 - \frac{\omega_h r}{\bar{a}_{s,\mathrm{pr}}(1 - \bar{M}_{s,\mathrm{pr}})} \tag{8}$$

The only difference between Eqs. (6) and (8) is a change in disturbance frequency from the primary to the harmonic frequency, which alters the overall phase value.

Linearized Disturbance Character

In reviewing Eqs. (5) and (6) for the lift and Eqs. (7) and (8) for the drag, it is clear that the upstream effect of the cylinder vortex shedding is the production of unsteady velocity disturbances in both the $\hat{\theta}$ and $\hat{r}$ coordinate directions, where these velocity disturbances propagate upstream at acoustic speeds. As illustrated in Fig. 6, however, far upstream of the cylinders the $\hat{r}$ and $\hat{\theta}$ cylindrical coordinates can be approximated by Cartesian $\hat{x}$ and $\hat{y}$ coordinates, respectively. In the cascade both the $\hat{x}$ and $\hat{y}$ Cartesian coordinates can be further related to the vane geometry itself, where the $\hat{x}$ coordinate is parallel to the vane chord and the $\hat{y}$ coordinate is normal to the vane chord. Therefore, using the Cartesian-coordinate approximation, the cascade vanes experience linearized velocity fluctuations caused by the downstream cylinders, where the linearized lift fluctuations are normal to the vane surfaces and the linearized drag fluctuations are parallel to the vane surfaces.

The phase lag of the induced velocity disturbances, as given by Eqs. (6) and (8), can also be linearized into Cartesian coordinates far upstream of the cylinders. As such, these phase lags can each be written as

$$\varphi_{p,h} = \varphi_0 - \frac{\omega_{p,h}(c - x)}{\bar{a}_{s,\mathrm{pr}}(1 - \bar{M}_{s,\mathrm{pr}})} \tag{9}$$

where Eq. (9) is valid for both primary and harmonic frequency disturbances. Equation (9) represents the analytical propagation model discussed in Ref. 12, and although this equation is derived using velocity disturbances the results are directly applicable to the concomitant, vane pressure response. In fact, the decomposed phase of the measured surface pressure, as given in Table 1, can be directly compared to the results of Eq. (9), as was done in Figs. 3 and 4.

Results

Phase Results

As already discussed, Figs. 3 and 4 show the decomposed phase of the vane unsteady pressure for the 0.475 inlet-Mach-number case; however, the overlaid curves in Figs. 3 and 4 can now be identified as the analytically computed phase derived from Eq. (9). Mach number values of 0.59 and 0.35, for the suction and pressure surfaces, respectively, were "optimized" in Eq. (9) to provide the curves shown in Figs. 3 and 4. These assumed Mach numbers were found to be in excellent agreement with the local vane Mach numbers derived from time-averaged cascade surface-pressure data.[12,14] Good agreement between the decomposed and analytically computed phase data, as well as the agreement between the assumed and local Mach numbers over the pressure and suction surfaces of the vanes, was found for all inlet Mach-number cases. This agreement essentially verifies that the cylinder forcing produces acoustically propagating potential disturbances consistent with the derived analytical models.

Amplitude Results

The rms unsteady pressure of the raw, rearward-forced, ensemble-averaged pressure-response signals was computed at each inlet Mach number tested, as shown in Fig. 7. The rms pressures given in Fig. 7 are to be measured from the displayed vane surface (suction or pressure) to the indicated symbols. These rearward-forced rms data can be compared to the forward-forced rms data given in Fig. 8; the forward-forced data were taken from the raw, ensemble-averaged pressure-response signals collected with the forcing cylinders 0.80 vane chords upstream of the vane row.[13] A comparison between Figs. 7 and 8 reveals the rms pressures to be on the same order for both forcing configurations, where the forward-forcing response is caused by both downstream-propagating potential and vortical disturbances.

The rearward-forced decomposed amplitudes, for both the primary and harmonic frequencies at all four inlet Mach numbers, are

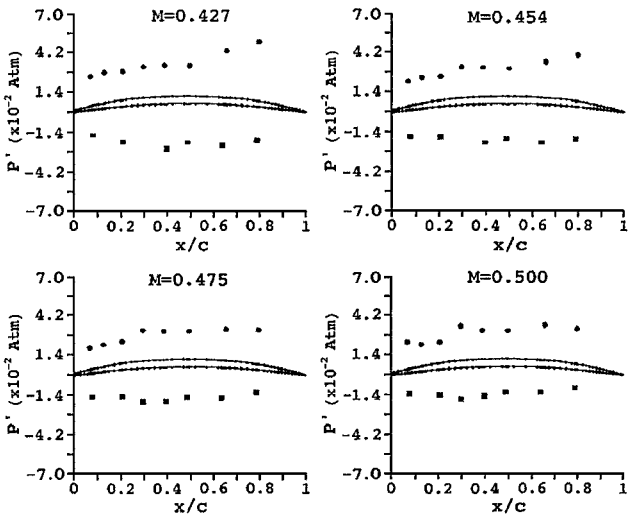

Fig. 7 RMS unsteady pressures for rearward forcing.

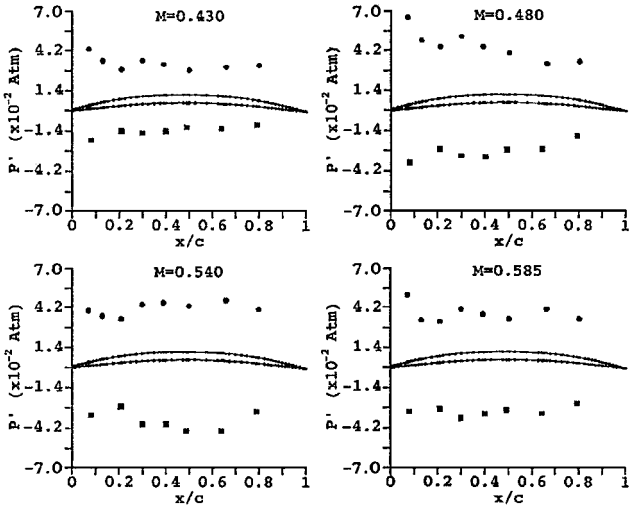

Fig. 8 RMS unsteady pressures for forward forcing.

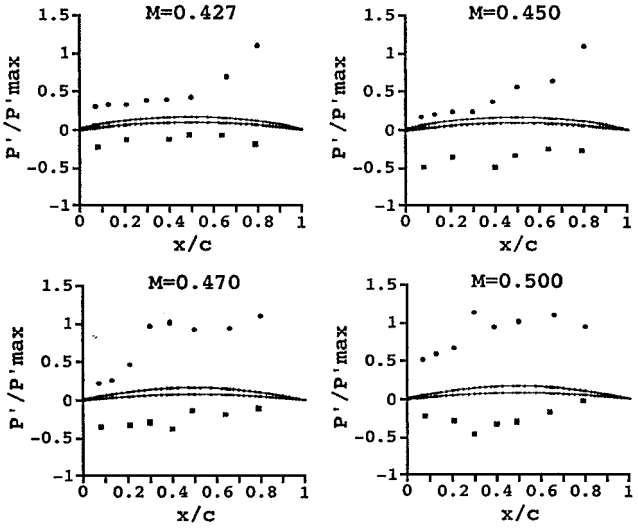

Fig. 9 Normalized, unsteady pressure amplitude for the fundamental frequency, rearward forcing.

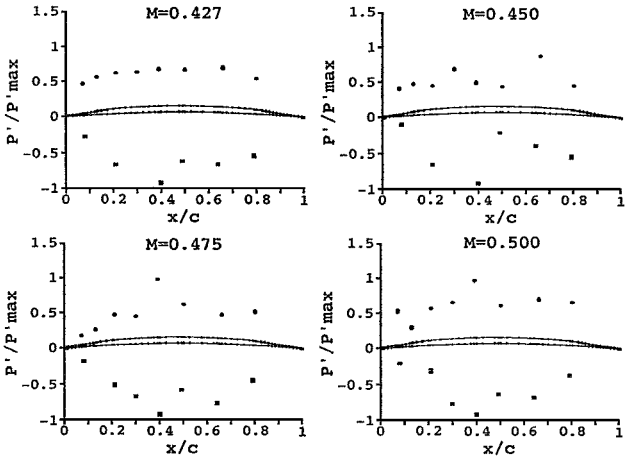

Fig. 10 Normalized, unsteady pressure amplitude for the harmonic frequency, rearward forcing.

shown in Figs. 9 and 10, respectively. If the rms data of Fig. 7 are compared to the amplitude data of Figs. 9 and 10, two important characteristics emerge. First, even though the pressure-transducer locations were limited at the vane trailing edge to the $x/c = 0.80$, extrapolation of the primary-frequency amplitude data in Fig. 9 from the $x/c = 0.80$ location to the trailing edge suggests a large trailing-edge unsteady-pressure rise. Second, pressure amplification near the $x/c = 0.30$ suction-surface location, in both Figs. 9 and 10, appears to be Mach number related and therefore possible evidence of "acoustic blockage."

Trailing-Edge Pressure Disturbance

The forward-forced rms data of Fig. 8 show a canonical decrease in amplitude toward the vane trailing edge for both the pressure and suction surfaces. Figure 8 also shows the familiar leading-edge singularity behavior expected for vortical disturbance interaction with the vane row. The trailing-edge pressure decrease in Fig. 8 is an expected response feature in agreement with the traditional notion of the Kutta condition for unsteady flows. The harmonic-frequency data of Fig. 10 also exhibit this expected trailing-edge response. Unexpectedly, however, singularity-like characteristics (i.e., similar to the leading-edge behavior of the forward-forced rms data of Fig. 8) are present near the trailing edge in the primary-frequency data of Fig. 9 at all four inlet Mach numbers. Moreover, the rearward-forced data of Figs. 9 and 10 both show a distinctive lack of a leading-edge singularity, unlike the forward-forced data of Fig. 8.

To our knowledge, the suggestion of a large trailing-edge pressure disturbance, as shown in Fig. 9, is the first experimentally observed occurrence of the phenomenon. This observation, in conflict with conventional wisdom, raises the question as to whether or not such a pressure rise near the trailing edge is theoretically forbidden, as is generally believed. Close examination of the literature reveals that the prohibition of a trailing-edge pressure rise appears to have been a choice rather than an absolute. This choice was based on previous notions of the Kutta condition, particularly for downstream-propagating disturbances interacting with a vane row. In fact, the forward-forced pressure data of Fig. 8 are in agreement with these views. Additionally, when upstream-propagating disturbances were considered this theoretical choice was also successful in predicting some characteristics of receptivity, in which the disturbances interact with a shear layer developed at the vane trailing edge.

An extensive review of Ref. 16 now suggests that a trailing-edge pressure rise may not be theoretically forbidden. In Ref. 16 Crighton and Leppington discuss the possibility of a trailing-edge pressure rise for the case in which upstream-propagating disturbances interact with a trailing-edge shear layer, as well as the case where disturbances interact with a trailing edge having matched upper and lower surface velocities. For the shear-layer case not allowing a large unsteady-pressure disturbance at the trailing edge requires a sinuous deflection of the shear layer.[16] For the matched velocity case, in which the current investigation can be categorized, multiple theoretical flow solutions are possible; however, only one solution rejects the possibility of a trailing-edge rise.[16] It is this solution, which rejects a trailing-edge pressure increase, that is generally accepted as correct. The remaining solutions are neglected on the basis that they do not satisfy the Kutta condition, even though the validity of choosing a Kutta-condition solution is "far from being satisfactorily resolved."[16] In fact, a rigorous demonstration of the validity of the Kutta condition for such flows has yet to be performed.[16]

It is instructive to consider the possible reasons why the primary-frequency data in Fig. 9 suggest a trailing-edge pressure rise, while the harmonic-frequency data of Fig. 10 do not. As already mentioned, a primary-frequency disturbance far upstream of the forcing cylinders fluctuates normal to the vane surfaces, whereas a harmonic-frequency disturbance fluctuates parallel to the vane surfaces. Only a disturbance with a surface-normal velocity component could have the possibility of producing a trailing-edge pressure rise, as discussed in Ref. 16.

Acoustic Blockage

The amplification of unsteady pressure near the $x/c = 0.3$ location in Figs. 9 and 10 may be the first experimental evidence of a recently proposed, subsonic amplification mechanism, which

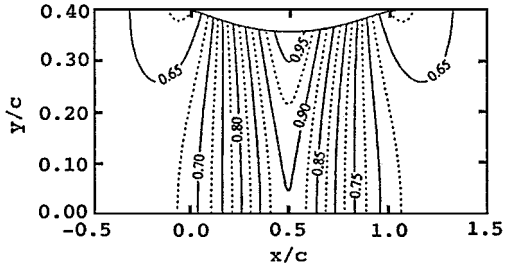

a) Laval-nozzle Mach-number contours

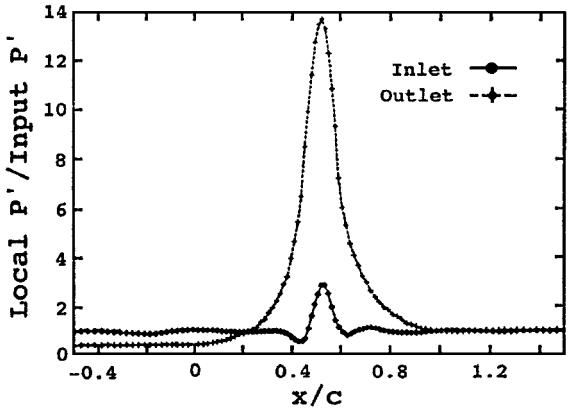

b) Unsteady surface-pressure amplitude

Fig. 11 Effect on unsteady surface-pressure response caused by forward and aft traveling disturbances in a near-sonic laval nozzle, with permission.[17]

Atassi et al.[17] termed "acoustic blockage." According to Atassi et al.,[17] potential waves traveling upstream from the trailing edge of a vane, in a subsonic flow, may be impeded in their upstream progress by the velocity of the oncoming flow. As the subsonic flow around the vane builds in Mach number, depending upon the frequencies and wavelengths, these waves can coalesce and amplify near the maximum local-Mach-number location along the vane. Disturbance amplifications of up to 20 times the incoming disturbance amplitude are theoretically possible for local Mach numbers approaching 0.99.

Figures 11a and 11b, taken with permission from Ref. 17, show results from a previous computational investigation of acoustic blockage. In particular, Fig. 11a shows Mach-number contours for a Laval nozzle, where the nozzle input velocity achieves near-sonic, but fully subsonic, conditions at the throat. Figure 11b shows unsteady-pressure results, sampled at multiple locations along the nozzle surface, in which unsteady potential disturbances are input and allowed to propagate, from both upstream and downstream in the nozzle. Note that the results of Fig. 11b correspond to the conditions of Fig. 11a and are normalized by the input disturbance amplitude. For the upstream-traveling potential disturbance in Fig. 11b, an amplification of nearly 14 times occurs at the maximum Mach-number location in the nozzle. Moreover at a position where the Mach number is as small as $\sim$0.7, noticeable amplifications of $\sim$1.4 can still be observed.

The pressure amplifications noted on the cascade vanes in Figs. 9 and 10 occur at the maximum Mach-number location on the suction surface of the vanes. Furthermore, although this amplification appears in all of the inlet-Mach-number cases, it is largest at the highest inlet-Mach-number case (0.500), where the maximum local Mach number over the vanes was 0.73. Because the pressure amplifications occur at the maximum local-Mach-number location and the maximum local Mach numbers correspond to those of Ref. 17, it can be argued that the data of Figs. 9 and 10 appear to provide suggestive evidence of acoustic blockage. These data further imply, as Atassi et al. predicted, that these amplifications can become important at relatively low Mach numbers, as amplifications are noticeable in Figs. 9 and 10 for maximum local Mach numbers near $\sim$0.6. Prior to the work of Atassi et al., such unsteady-pressure amplifications had always been assumed to be associated with transonic flows and oscillating shocks; acoustic blockage provides a fully subsonic mechanism for providing similar-order amplifications.

Conclusions

This paper has presented raw and frequency-decomposed unsteady pressure-response data from the turning vanes of an unsteady, compressible linear cascade, over inlet Mach numbers from 0.427 to 0.500. Unsteady forcing of the cascade was generated downstream of the vane row and was potential in nature. The obtained pressure-response data allowed for unambiguous interpretation, as the measured disturbances were confirmed to originate downstream at the forcing cylinders and propagate upstream at acoustic speeds into the oncoming compressible flow. These disturbances appear to have possibly elicited two new types of pressure-response amplification mechanisms, including a trailing-edge unsteady-pressure rise and a subsonic amplification mechanism known as acoustic blockage. The effects of both of these amplification mechanisms are large, even at the relatively low Mach numbers investigated. Moreover, if these effects are physically relevant, as is the case for the present data, the amplification mechanisms are clearly of first-order importance to the rotor/stator and stage-to-stage interaction problems.

In closing, it should be noted that this paper is not intended to be the definitive work in this area or of particular use in designing new stator vanes. It is merely the first step in an investigation of two, possibly new, pressure amplification mechanisms in cascade flows. The investigation suffers from Mach-number limitations inherent to the cascade configuration, such that unsteady forcing up to inlet Mach numbers of only 0.500 were possible for rearward forcing. Also, because of their minimal thickness, the aft surface-pressure measurement locations were limited to $x/c = 0.80$. Moreover, the cascade forcing mechanism is not directly analogous to that of an actual compressor, where the source of unsteady forcing is rotating. Given these limitations, however, there remains no evidence to suggest that the behavior of the obtained surface-pressure data should be characterized as anomalous. At the very least, these cascade results provide the mere possibility of two new unsteady-pressure amplification mechanisms; the results of which should be taken seriously, as well as addressed further in an actual engine flowfield.

Acknowledgments

This research effort was jointly sponsored by the Turbine Engine Division of the Aero Propulsion and Power Directorate at Wright–Patterson Air Force Base, the Aerospace and Mechanical Engineering Department at the University of Notre Dame, the Department of Aeronautics at the U.S. Air Force Academy, and the Indiana Space Grant Consortium.

References

[1] Thomson, D., "The National High Cycle Fatigue (HCF) Program," *Proceedings of the 3rd National Turbine Engine High Cycle Fatigue Conference*, San Antonio, TX, Feb. 1998.

[2] Schmidt, D. P., and Okiishi, T. H., "Multistage Axial-Flow Turbomachine Wake Production, Transport, and Interaction," *AIAA Journal*, Vol. 15, No. 8, 1977, pp. 1138–1145.

[3] Dring, R. P., Joslyn, H. D., and Hardin, L. W., "Investigation of Axial Compressor Rotor Aerodynamics," *Journal of Engineering for Power*, Vol. 104, No. 1, 1982, pp. 84–96.

[4] Zierke, W. C., and Okiishi, T. H., "Measurement and Analysis of Total-Pressure Unsteadiness Data from an Axial-Flow Stage," *Journal of Engineering for Power*, Vol. 104, No. 2, 1982, pp. 479–488.

[5] Gallus, H. E., Lambertz, J., and Wallmann, T., "Blade-Row Interaction in an Axial Flow Subsonic Compressor Stage," *Journal of Engineering for Power*, Vol. 102, No. 1, 1980, pp. 169–177.

[6] Fleeter, S., Jay, R. L., and Bennett, W. A., "Rotor Wake Generated Unsteady Aerodynamic Response of a Compressor Stator," *Journal of Engineering for Power*, Vol. 100, No. 4, 1978, pp. 664–675.

[7] Johnston, R., and Fleeter, S., "Time-Resolved Variations of an IGV Flow Field in the Presence of a Rotor Potential Field," AIAA Paper 96-2670, July 1996.

[8] Johnston, R., and Fleeter, S., "Three-Dimensional Time Resolved Measurements of IGV-Rotor Potential Interactions," AIAA Paper 98-3896, July 1998.

[9]Hsu, S. T., and Wo, A. M., "Near-Wake Measurement in a Rotor/Stator Axial Compressor Using Slanted Hot-Wire Technique," *Experiments in Fluids*, Vol. 23, No. 5, 1997, pp. 441–447.

[10]Probasco, D. P., Wolff, J. M., Copenhaver, W. W., and Chriss, R. M., "Unsteady Blade Row Potential Interaction in a Compression Stage," AIAA Paper 97-3285, July 1997.

[11]Probasco, D. P., Wolff, J. M., Copenhaver, W. W., and Chriss, R. M., "Axial Spacing Effects in a Transonic Compressor on the Upstream Vane Loading," AIAA Paper 98-3431, July 1998.

[12]Fabian, M. K., and Jumper, E. J., "Rearward Forcing of an Unsteady Compressible Cascade," *Journal of Propulsion and Power*, Vol. 15, No. 1, 1999, pp. 23–30.

[13]Fabian, M. K., and Jumper, E. J., "Convected and Potential Unsteady Disturbances Interacting with an Unsteady Cascade," AIAA Paper 96-2672, July 1996.

[14]Fabian, M. K., "Unsteady Pressure Distributions Around Compressor Vanes in an Unsteady, Transonic Cascade," Ph.D. Dissertation, Dept. of Aerospace and Mechanical Engineering, Univ. of Notre Dame, South Bend, IN, Dec. 1995.

[15]Oates, G. C., *Aerothermodynamics of Gas Turbine and Rocket Propulsion: Revised and Enlarged*, AIAA Education Series, AIAA, Washington, DC, 1988, p. 405.

[16]Crighton, D. G., and Leppington, F. G., "Radiation Properties of the Semi-Infinite Vortex Sheet: the Initial-Value Problem," *Journal of Fluid Mechanics*, Vol. 64, Pt. 2, 1974, pp. 393–414.

[17]Atassi, H. M., Fang, J., and Ferrand, P., "A Study of the Unsteady Pressure of a Cascade Near Transonic Flow Condition," American Society of Mechanical Engineers, Paper 94-GT-476, June 1994.